Journal of Drug Delivery Science and Technology 106 (2025) 106704

Contents lists available at ScienceDirect

Journal of Drug Delivery Science and Technology

journal homepage: www.elsevier.com/locate/jddst

A comprehensive study on needle-free injection technology combined with midazolam nanosuspension

He Zhang [a,b,1], Jiarui Chen [c], Xiaolu Han [a], Liang Xu [a], Zengming Wang [a], Nan Liu [a], Yang Yang [a,*], Hui Zhang [a,**], Ai-ping Zheng [a]

[a] State Key Laboratory of Toxicology and Medical Countermeasures, Beijing Institute of Pharmacology and Toxicology, Beijing, 100850, China
[b] Department of Pharmacy, The 909th Hospital, Zhangzhou, 363000, China
[c] School of Pharmacy, North China University of Science and Technology, Tangshan, 063000, China

ARTICLE INFO

Keywords:
Needle-free
Jet injection
Nanosuspension
Nanocrystal
Midazolam

ABSTRACT

Needle-Free Injection Technology (NFIT), which administers medication through a high-pressure transdermal jet, is limited to a delivery volume of no more than 1 mL due to device constraints. This poses challenges for the administration of poorly water-soluble drugs. Despite its potential for intramuscular delivery of nanocrystal drugs, research in this area is scarce, particularly regarding the exploration of the injection process and outcomes at the intramuscular depth. We developed solution and nanosuspension formulations of the poorly water-soluble drug midazolam and assessing their effectiveness following NFIT and needle injection administration. Our systematic evaluations encompass the velocity of needle-free injection, the establishment of a gel model for visualizing distribution, and documentation of the needle-free injection process, distribution range, impact of needle-free injection on nanocrystals' size and tissue injury, as well as a comprehensive pharmacokinetic study. Our systematic evaluation confirmed that the nanocrystals retained their physicochemical properties following needle-free injection, ensuring consistent therapeutic efficacy. A significant finding was the faster time to maximum concentration (T_{max}) observed with the NFIT-administered nanosuspension (11.67 ± 5.16 min) compared to both the needle injection of nanosuspension (32.50 ± 22.08 min) and the NFIT-administered solution (32.50 ± 14.75 min). Additionally, the needle-free method extended the residence time of the nanosuspension formulation. This research enhanced our understanding of NFIT and underscored its synergistic potential when combined with nanosuspensions for intramuscular drug delivery. Our findings present NFIT as a viable, less injury and rapidly effective alternative to traditional needle injections, especially offering a promising approach for the administration of midazolam nanosuspension.

1. Introduction

Needle-Free Injection Technology (NFIT) refers to the process of utilizing a pressure source to generate instantaneous high pressure, causing the medications to form a high-velocity, high-pressure jet stream through a nozzle. This stream penetrates the skin to reach an appropriate depth for absorption and therapeutic efficacy. NFIT is capable of delivering solutions, powders, and depot formulations. Compared to traditional needle injection, NFIT effectively mitigates injection-related pain, reduces risk of accidental needlestick injuries and addresses needle-phobia [1]. The simplicity of needle-free injectors allows for easy use by patients or individuals in emergency, facilitating intradermal, subcutaneous, and intramuscular injections for localized or systemic therapeutic effects. The injection process is characterized by high safety, ensuring efficient delivery, precise dosing, and accelerated absorption with the medication being uniformly dispersed. NFIT is gaining increasing attention from researchers as an alternative to needle injection in certain fields. However, the typical limitation of NFIT is the volume per injection, typically below 1 mL, which poses challenges for the administration of poorly water-soluble drugs that often require larger volumes for effective dosing [2]. The existing research on NFIT has primarily focused on the subcutaneous administration of

* Corresponding author.
** Corresponding author. 27th Taiping Road, Haidian District, Beijing, 100850, China.
E-mail address: zhengap@bmi.ac.cn (H. Zhang).
[1] First author.

https://doi.org/10.1016/j.jddst.2025.106704
Received 10 November 2024; Received in revised form 26 January 2025; Accepted 10 February 2025
Available online 20 February 2025
1773-2247/

medications, including vaccines [3–5], insulin [6–8], hormones [9,10], certain nanomedicines [11–18] and so on.

Midazolam, a benzodiazepine with poor water solubility, is recognized for its multifaceted pharmacological profile, which encompasses anti-anxiety, muscle relaxant, anticonvulsant, sedative, and hypnotic effects [19]. As a first-line treatment for status epilepticus, midazolam's intravenous administration is widely acknowledged [20]. However, for conditions like epilepsy that demand urgent intervention, the unpredictability and rapid response requirements can render conventional routes such as oral or rectal administration insufficient due to their delayed onset [21]. Additionally, the efficacy of nasal midazolam administration is subject to variability influenced by factors like the nasal mucosa's condition and the presence of secretions [22,23]. In scenarios where intravenous access is unavailable, needle-free intramuscular injection emerges as a stable, dependable, and swift alternative for midazolam delivery, providing a critical therapeutic option in emergency settings.

Several methods have been developed to improve the solubility of injectable formulations, including pH adjustment, salt formation, co-solvents and the use of surfactants. However, these methods are limited by their solubility, potential toxicity, and specificity [24]. Nanocrystals technology emerges as a vital approach to addressing the challenges associated with the small volume of NFIT required and limited dissolution and bioavailability of poorly water-soluble drugs like midazolam. At the nanoscale, drugs demonstrate increased loading capacities and possess significantly amplified specific surface areas [25]. This enhancement allows for a significant improvement in saturated solubility and dissolution rate. Furthermore, it extends the residence time of the drug within the body, leading to better therapeutic efficacy.

The current integration of NFIT with nanomedicine primarily aims to achieve drug delivery and investigate the impact of formulation characteristics and device parameters on injection outcomes. While the combination of nanosuspensions and NFIT has already established a foundation in subcutaneous applications, such as diclofenac nanosuspensions [18], there remains a gap in the research regarding their application for intramuscular delivery. Intramuscular injection, leveraging the muscle's rich vascular network and tolerance for larger volumes, is particularly beneficial for rapid drug absorption and achieving high drug concentrations in target tissues. Given the diffuse distribution characteristic of NFIT and the rapid absorption properties of nanocrystals, the combination of NFIT and nanocrystals for intramuscular delivery may offer enhanced therapeutic effects.

In this study, we developed and evaluated the NFIT for the intramuscular delivery of midazolam. Fig. 1 schematically illustrates our strategy of this study. By preparing both solution and nanosuspension formulations (50 mg/mL) and utilizing an optimized NFIT device (0.04–0.2 mL for intramuscular injection), we addressed the limitations posed by restricted injection volumes and contrasted the different forms of midazolam to assess its treatment effects. Our systematic evaluation encompasses the velocity of needle-free injection, the establishment of a model for intramuscular visualizing distribution, and documentation of the injection process, distribution range. Our evaluation also included an analysis of skin and tissues injury and nanocrystals' particle size caused by NFIT. Furthermore, through in vivo pharmacokinetic studies, we comprehensively analyzed the effects of NFIT on drug absorption kinetics. Our study demonstrates the synergistic effect of NFIT combined with midazolam nanosuspensions, which significantly enhances drug absorption rates and bioavailability while concurrently reducing injection-related injury. This approach introduces an innovative strategy for the administration of midazolam, providing a more rapid and patient-friendly delivery method.

2. Materials and methods

2.1. Materials

Midazolam was obtained from Yichang Humanwell Pharmaceutical Co., Ltd. (Yichang, China), and diazepam was purchased from Shandong Xinyi Pharmaceutical Co., Ltd. (Dezhou, China). Deoxycholic acid sodium salt (sodium deoxycholate, SDC) was a gift from Huzhou Zhanwang Pharmaceutical Co., Ltd. (Huzhou, China). PVP K25 was purchased from BASF (Berlin, Germany). 0.2 mm zirconia grinding beads for wet milling were acquired from Cenotec Co., Ltd. (South Korea). mPEG350 was a gift from Nanjing Well Pharmaceutical Group

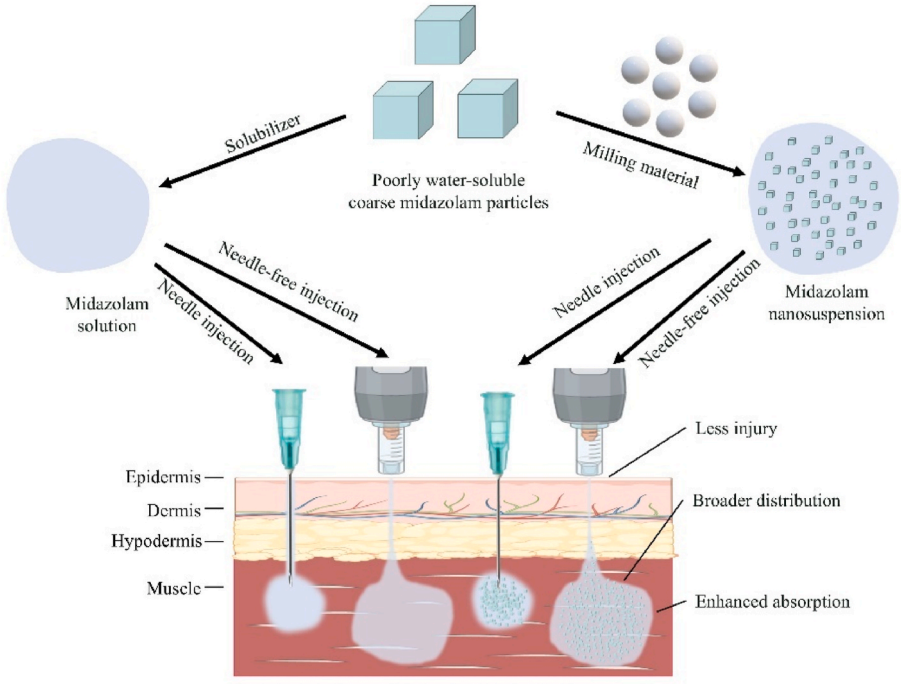

Fig. 1. Schematic overview of the study's main research approach and findings. This figure showcases our study on enhancing midazolam's solubility through liquid solubilization and wet media milling, comparing needle and needle-free injection methods for different formulations.

Co., Ltd. (Nanjing, China). Anhydrous ethanol, propylene glycol, and ammonium persulfate were procured from Sinopharm Group Co., Ltd. (China). LE agarose was sourced from SeaKem (Rockland, ME, USA), and acrylamide was purchased from Merck (Darmstadt, Germany). Bis-acrylamide, tetramethylethylenediamine (TEMED), and methylene blue were obtained from JSENB Genefist (China), and Energy Chemical (China) respectively. The needle-free injector (0.04–0.2 mL) for intramuscular injections was custom-made by Quinovare (Beijing, China). Thirty-day-old pig skin was provided by Aperture Biotechnology (Shandong, China). Gluta fixative was purchased from Leagene (Beijing, China). HPLC-grade methanol used in the high-performance liquid chromatography studies was sourced from Fisher Chemical (USA).

2.2. Preparation and rheological characterization of midazolam solution and nanosuspension

2.2.1. Midazolam solution

In the preparation of the midazolam solution, midazolam was first dissolved in anhydrous ethanol at a concentration of 5 % (w/w) with vigorous stirring. Following this, mPEG350 was introduced at a concentration of 42.25 % (w/w) and mixed thoroughly to achieve a homogeneous solution. Subsequently, propylene glycol was added at a 2 % (w/w) concentration. Finally, the remaining mPEG350 (22.75 % w/w) and water (23 % w/w) were mixed in, with continuous stirring to ensure complete dissolution of midazolam.

2.2.2. Midazolam nanosuspension

To prepare the midazolam nanosuspension, we initially prepared a solution containing 0.2 % (w/w) sodium deoxycholate (SDC) and 2.5 % (w/w) polyvinylpyrrolidone K25 (PVP-K25). Midazolam was then incorporated at a concentration of 5 % (w/w). The mixture was subsequently subjected to wet media milling using a DYNO®-MILL RESEARCH LAB mill (Willy A. Bachofen AG, Germany) to achieve a uniform particle size. The milling process involved the use of 0.2 mm zirconia grinding beads, operated at a speed of 3000 rpm for a duration of 30 min.

2.2.3. Viscosity and density determination

Viscosity measurements were performed using a Brookfield viscometer (model DVNXLV, USA) at a shear rate of 200 rpm with a CP-41 spindle, under a controlled temperature of 25 °C. This temperature was maintained throughout the tests to standardize the viscosity assessments. Concurrently, the density of each formulation was determined using a calibrated density bottle. The mass of a precisely measured volume of the formulation at 25 °C was used to calculate its density.

2.3. Characterization of midazolam nanocrystals

2.3.1. Particle size analysis

The particle size, zeta potential and polydispersity index (PDI) analysis of the prepared midazolam nanosuspension were diluted 200-fold with a 0.2 % SDC and determined by dynamic light scattering (DLS) through a Malvern ZS90 particle size analyzer (Malvern Panalytical, England). The system was set for 5 runs, each with a duration of 15 s and 3 measurements per run. The average particle size and standard deviation were obtained by fitting the data with a Gaussian function. For stability assessment, the prepared midazolam nanosuspensions were stored at room temperature (25 ± 2 °C), and their particle size, zeta potential and PDI were monitored at 0, 10, 20, 30 and 40 days to observe any changes.

2.3.2. Transmission electron microscope (TEM)

The morphological characteristics and particle size distribution of the midazolam nanocrystals were evaluated using a JEOL JEM-F200 transmission electron microscope (TEM) to gain insights into their physical properties. The TEM imaging was performed under an acceleration voltage of 200 kV, which provided high-resolution images of the nanocrystals. These images were essential for visualizing the shape and size of the particles. To quantitatively analyze the particle size distribution, the captured images were processed using ImageJ software, a widely-used tool for image analysis.

2.3.3. Dissolution behavior of midazolam nanosuspension

The dissolution behavior of the midazolam nanosuspension was evaluated by auto sampling dissolution (Wahyong instrument, Guangdong, China). Four groups, including the midazolam coarse powder, physical mixtures (midazolam, SDC, and PVP-K25), solution and nanosuspension, were diluted to10 μg/mL by phosphate-buffered saline (PBS; pH 7.4). The drug was then released at 37 °C in 900 mL of PBS using a dissolution apparatus. At each time point, 10 mL of the sample was centrifuged to prevent any undissolved nanocrystals, and then take the supernatant for measurement. The samples were characterized by high-performance liquid chromatography. The analysis was performed on a ZORBAX RX-C18 system (5 μm, 4.6 × 150 mm, Agilent, Santa Clara, USA) at 25 °C. The mobile phase was a methanol-phosphate buffer solution (dissolved 0.1 mol/L phosphate and 0.03 mol/L trimethylamine in 1000 mL water, adjusted to pH 3.5 with 0.1 mol/L sodium hydroxide) (65:35, v/v) at a flow rate of 1.0 mL/min. The detection wavelength was 220 nm, and the injection volume was 10 μL.

2.4. Construction and utilization of an injection phantom model for visualization

The gel model was meticulously designed to replicate the maximal thicknesses of human skin layers. The epidermal, dermal, and subcutaneous layers were represented with thicknesses of 2.4 mm, 5.9 mm, and 5.9 mm, respectively, while the muscle layer was modeled at a thickness of 40.0 mm. LE agarose, prepared at concentrations of 0.7 %, 0.3 %, and 1.4 % (w/w) for the muscle, subcutaneous, and dermal layers, respectively, was employed to achieve these dimensions. The agarose solutions were heated in a microwave to ensure complete dissolution and then sequentially poured into molds to form layers, with each layer being added before the previous one fully solidified to prevent interface separation. To simulate the epidermal layer, a 33 % polyacrylamide gel was prepared using a mixture of 30 % acrylamide and 3 % bis-acrylamide. The mixture was combined with distilled water and 1.5 × Tris-HCl buffer to achieve the desired final concentration. Polymerization was initiated by adding 10 % ammonium persulfate and 1 % TEMED [26].

2.5. Visualization of microjet penetration and dispersion

Visualization of the needle-free injection process was accomplished by a high-speed camera Phantom V311 (Vision Research Inc., Phantom) in conjunction with a Nikon lens. The lighting system, powered by a 2000 W halogen lamp, ensured clear and flicker-free footage. The camera was set to a sampling frequency of 10,000 frames per second (fps) with a sampling period of 100.00 μs and an exposure time of 4 μs, capturing a sequence of continuous images at a resolution of 640 × 480 pixels. To enhance contrast, a white background was utilized, and the injection solution was dyed with methylene blue at a concentration of 1 % w/w. The Phantom Camera Control (PCC) software was employed for analyzing injection velocity, duration, and the distribution process within the gel at a volume of 0.2 mL. The injection velocity was determined using the two-point method within the PCC software, providing precise measurements of the injection dynamics.

2.6. Assessment of NFIT delivery across the skin

2.6.1. Particle size of nanocrystals

The Franz diffusion cell technique was employed to assess changes in

nanocrystals size post-injection through 30-day-old Bama miniature skin. The skin specimens, measuring 2 cm by 2 cm, were mounted onto the injection port of the Franz cell, secured by an iron mesh above the receptor chamber. Following injection using a needle-free injector, the post-injection nanosuspension was collected for analysis. Malvern ZS90 was utilized to measure the particle diameter before and after the transdermal injection, ensuring the evaluation of any alterations in the nanosuspension's particle size distribution.

2.6.2. Cryo-scanning electron microscopy (Cryo-SEM)

Porcine skin penetration was performed using both a needle-free injector and a 29G insulin syringe (Becton, Dickinson and Company). Following penetration, the skin samples were fixed with a 2.5 % glutaraldehyde solution to preserve their structure. Subsequent examination of the samples was conducted using a cryo-scanning electron microscope (Hitachi Regulus 8100, Japan) at an acceleration voltage of 3.0 kV. This analysis allowed for the visualization and measurement of the skin lesions induced by the injections. The diameter and area of these lesions were quantified utilizing ImageJ software, providing an assessment of the injection impact on the skin tissue.

2.6.3. Hematoxylin and Eosin (HE) staining

To evaluate the muscle cell injury caused by needle injection and needle-free injection, we utilized a needle-free injector and a 29G insulin syringe. Rabbit right leg tissue was selected as a negative control, while the left leg muscle tissue was injected with saline and 1.7 % acetic acid, respectively. The 1.7 % acetic acid was used to enhance the irritancy of the different delivery methods. Sampling was performed 5 min after injection and the tissue morphology was observed after HE staining.

2.7. Pharmacokinetic study

Male Sprague-Dawley rats (250–270g) were obtained from SPF Biotechnology Co., Ltd., Beijing, China, for a pharmacokinetic study approved by the Animal Laboratory of the Laboratory Animal Center, Academy of Military Medical Sciences (ethics code permit no. IACUC-DWZX-2025-511). Twenty-four rats were randomly assigned to four groups (n = 6 per group) and acclimatized to a controlled environment with a temperature of 25 ± 2 °C, 40%–60 % relative humidity, and a 12-h light/dark cycle, with free access to food and water for one week. Fasting was imposed for 12 h before the experiment, with water available ad libitum. All procedures were conducted to minimize animal distress and the number of animals used. Isoflurane anesthesia was administered for injection and blood collection. Rats received one of four treatments via intramuscular injection: needle solution (N-S), needle-free solution (NF-S), needle nanosuspension (N-N), or needle-free nanosuspension (NF-N), each at a dosage of 1 mg/kg. Blood samples (0.3 mL) were collected at various time points post-administration (2 min, 5 min, 15 min, 30 min, 1 h, 1.5 h, 3 h, 6 h, 9 h, and 12 h) via the ocular venous plexus into heparinized tubes. After centrifugation at 4 °C at 6000 rpm for 10 min, the serum was separated and collected for analysis. Protein precipitation was induced with 0.1 % ethyl acetate in acetonitrile, followed by vortex mixing for 30 s and centrifugation at 14000 rpm for 10 min. The supernatant was analyzed using HPLC.

2.8. Quantitative determination of midazolam in plamas

Quantitative analysis of midazolam was performed using an UltiMate™ 3000 HPLC system equipped with Chromeleon 7 software (Thermo Fisher Scientific, MA, USA). Detection was achieved with a UV detector set at 220 nm. The composition of the mobile phase is consistent with that used in section 3.3.4. Chromatographic separation was performed on an Alphasil ES-C18 column (5 μm particle size, 2.1 mm inner diameter × 100 mm length, Acchrom, Beijing, China) at a flow rate of 0.2 mL/min, with an injection volume of 10 μL and a column temperature maintained at 40 °C. Calibration of the HPLC method was achieved using a series of midazolam standard solutions prepared in blank serum, with diazepam at a concentration of 500 ng/mL serving as the internal standard. The resulting calibration curve exhibited linearity over the concentration range of 10–400 ng/mL. The assay's sensitivity was confirmed by a lower limit of detection at 5 ng/mL and a lower limit of quantification at 10 ng/mL, ensuring the accuracy and reliability of midazolam quantification.

2.9. Statistical analysis of data

Results are presented as the mean ± standard deviation. Statistical comparisons between two groups were performed using Student's t-test, with a p-value ≤ 0.05 defining statistical significance. Image analysis was conducted using ImageJ software (National Institutes of Health, Maryland, USA), which facilitated the quantitative assessment of visual data. Pharmacokinetic modeling and data analysis were performed utilizing Phoenix WinNonlin® version 8.3.5 (Certara, Delaware, USA), a comprehensive tool designed for the analysis of pharmacokinetic and pharmacodynamic data. Furthermore, the statistical evaluation of in vivo experimental data was carried out with GraphPad Prism version 8 (San Diego, CA, USA), which provided a robust platform for data interpretation and graphical representation.

3. Results and discussion

3.1. Preparation and characterization of midazolam solution and nanosuspension

The midazolam solution was prepared by dissolving the drug in a mixture of anhydrous ethanol and mPEG350, followed by the incorporation of propylene glycol and the remaining solvents to achieve a homogeneous solution. The nanosuspension was fabricated using a top-down wet media milling technique, which resulted in a fine dispersion of midazolam nanocrystals within a matrix of SDC and PVPK25. This method was selected for its efficiency in reducing particle size, which is essential for improving the bioavailability of poorly water-soluble compounds.

3.1.1. Rheological characterization

The factors that influence the dispersion and penetration characteristics of needle-free injection encompass the chemical attributes of the injected medication, the velocity profile of the microjet, as well as the mechanical properties of the medium being penetrated [27]. In our study, we primarily analyzed the impact of physicochemical factors of drugs on the process and in vivo distribution of needle-free injections through in vitro experiments, providing corresponding analytical support for in vivo pharmacokinetic experiments.

We conducted rheological assessments to ensure the compatibility of the midazolam formulations with needle-free injectors and to elucidate the factors influencing injection distribution, thereby providing a rationale for subsequent evaluation of the injection process. The rheological attributes of the midazolam solution and nanosuspension were characterized to ensure their suitability for NFIT and gain insights into the factors that influence injection distribution. The viscosity of the midazolam solution was measured at 23.55 ± 1.31 cP, significantly higher than that of the nanosuspension, which registered 2.35 ± 0.11 cP (n = 3). Concurrently, the density of the solution and nanosuspension formulations was determined to be 1.11 ± 0.001 g/mL and 1.01 ± 0.02 g/mL (n = 3), respectively. Under the same delivery energy, viscosity and density jointly influence the shape of drug dispersion within the tissue after needle-free injection [28]. These parameters are pivotal as they provide critical support in elucidating the injection process, the spatial distribution after injection, and the subsequent pharmacokinetic profiles.

3.1.2. Characterization of midazolam nanosuspension

3.1.2.1. Particle size. Based on the Noyes-Whitney equation, the dissolution rate of nanocrystals is closely related to their particle size: as the particle size decreases, the surface area increases accordingly, thereby accelerating the dissolution rate. To understand the particle size characteristics of midazolam nanocrystal suspension, DLS was employed to determine the particle size and zeta potential of midazolam nanocrystals using a Malvern ZS90 particle size analyzer. The zeta potential, a key parameter reflecting colloidal stability and resistance to aggregation, was measured at −40.9 ± 3.18 mV, suggesting a stable dispersion with minimal aggregation tendency. The average particle size was determined to be 186.27 ± 3.43 nm as shown in Fig. 2 (a), which is optimal for improving the dissolution rate and bioavailability of poorly water-soluble drugs.

3.1.2.2. TEM. To gain a deeper understanding of the morphological characteristics of midazolam nanocrystals and to verify the accuracy of DLS technology in particle size detection, we employed TEM technology for further observation and analysis. The particle size measurements and representative TEM images of the midazolam nanocrystals are depicted in Fig. 2 (b). The particle size distribution, measured at 190.06 ± 0.85 nm, corroborated well with the DLS, thereby further confirming the consistency and stability of the midazolam nanocrystals' size characteristics.

3.1.2.3. Dissolution behavior of midazolam nanosuspension. To evaluate the solubilization effect of midazolam nanosuspension prepared through nanocrystal technology, predict its bioavailability in vivo, simulate the dissolution process of the drug in vivo, we investigated the dissolution behavior of midazolam active pharmaceutical ingredient (API), physical mixtures, and nanosuspensions. The results in Fig. 2 (c) indicate that the prepared midazolam nanosuspension was almost completely dissolved (99.23 %) within 10 min, with a dissolution rate significantly superior to that of midazolam API (0.77 %) and the physical mixture group (2.15 %). The dissolution rate and particle size of the midazolam nanosuspension conformed to the Noyes-Whitney equation, where smaller particle size results in a larger relative surface area and faster release rate [29].

3.1.2.4. Stability assessment. Midazolam nanosuspensions were stored at ambient conditions (25 ± 2 °C) and analyzed at intervals over a 40-day period to assess the short-term physical stability. Both particle size and PDI were monitored, and the results indicated that the nanosuspensions retained their physical stability and homogeneity. These findings are further illustrated in Fig. 2 (d) with no significant changes in these parameters observed throughout the study period.

3.2. Characterization of the needle-free injection process

3.2.1. Injection process observation in air

To gain comprehensive insights into the NFIT and the dynamics of drug ejection, we assessed the behavior of high-velocity jets in air (Fig. 3), thereby providing a rationale for the efficacy of needle-free injections. The initial phase of the needle-free injection process was captured using a high-speed camera to analyze the ejection dynamics in air. The results indicated that the midazolam solution exhibited a velocity of 130.96 ± 5.22 m/s with a duration of 121.76 ± 11.69 ms, whereas the nanosuspension demonstrated a slightly lower velocity of 107.65 ± 2.65 m/s and a longer duration of 142.06 ± 5.12 ms (n = 5). Recent studies have shown that during needle-free injection, high-viscosity liquids can generate a "viscous heating" effect [30]. This effect occurs due to the shear friction between fluid layers during high-speed flow, which produces heat and leads to localized temperature increases and a reduction in viscosity. In our experiments, the nozzle material used was polycarbonate, which has a low thermal conductivity. This material retains more heat in the outer layer of the jet,

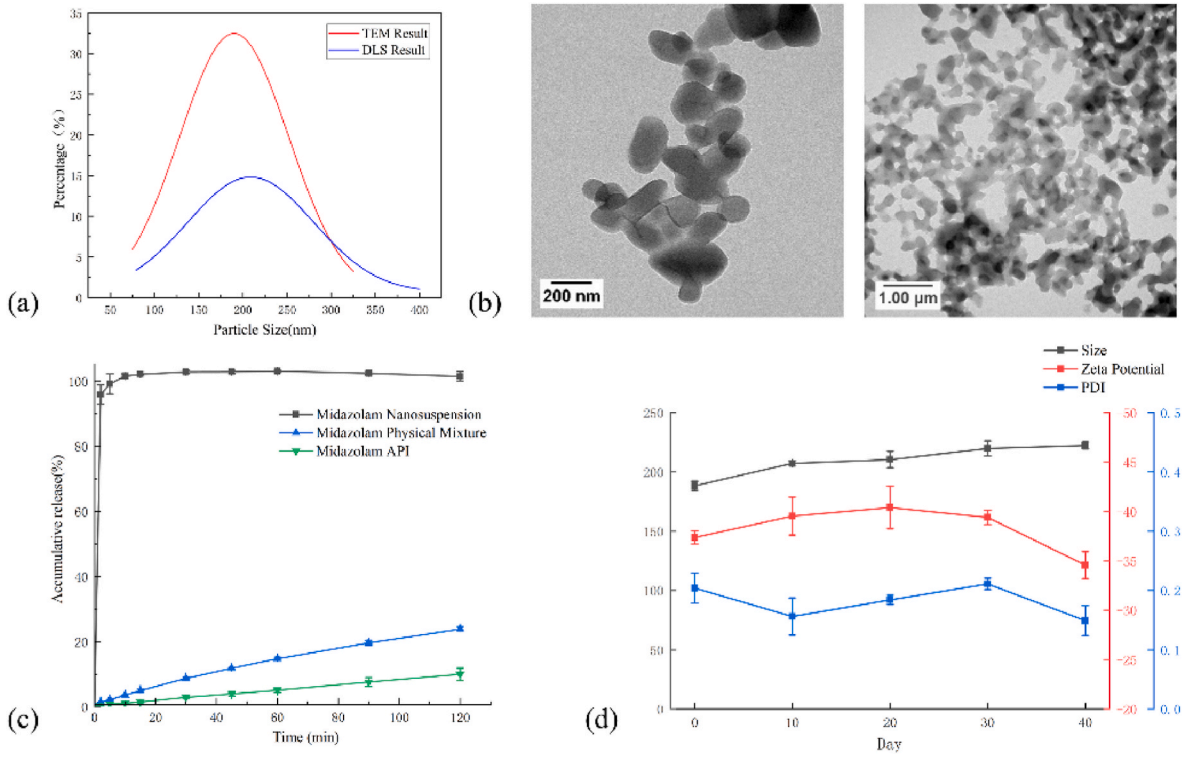

Fig. 2. Characterization of midazolam nanosuspension: (a) particle size distribution analyzed by dynamic light scattering (DLS) and transmission electron microscopy (TEM); (b) TEM images at a scale bar of 200 nm and 1 μm; (c) dissolution behavior of midazolam nanosuspension, physical mixture and active pharmaceutical ingredient; (d) stability assessment of midazolam nanosuspension in 40 days.

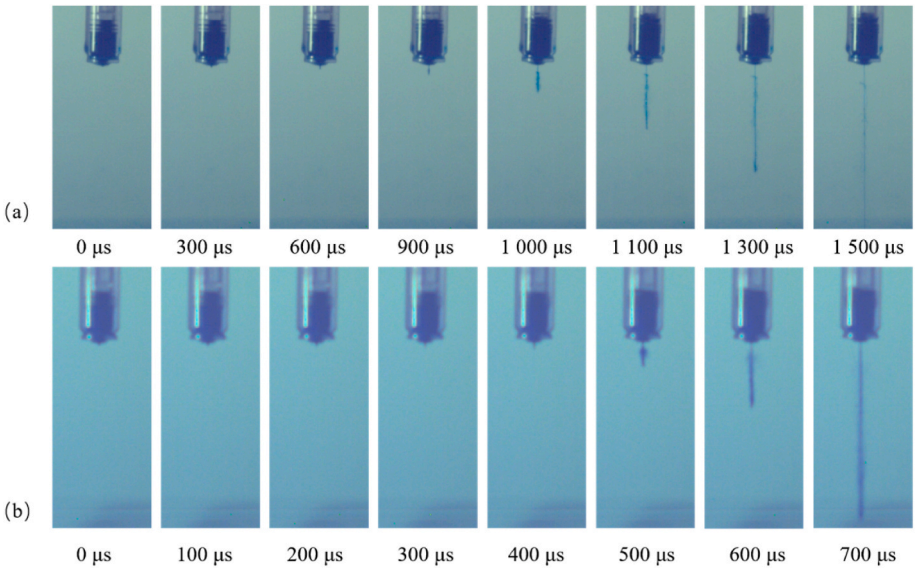

Fig. 3. Initial stages of needle-free injection of different formulations in air. (a) midazolam solution, (b) midazolam nanosuspension. The midazolam solution exhibited a velocity of 130.96 ± 5.22 m/s with a duration of 121.76 ± 11.69 ms, whereas the nanosuspension demonstrated a slightly lower velocity of 107.65 ± 2.65 m/s and a longer duration of 142.06 ± 5.12 ms (n = 5).

thereby increasing the jet velocity. The viscosity range reported in the literature is 1–1000 cP. In our study, the viscosity of the solution formulation (23.55 cP) is higher than that of the nanosuspension (2.35 cP), making it a high-viscosity fluid. Due to the viscous heating effect, the local temperature of the high-viscosity fluid increases, reducing its viscosity and potentially increasing its flow rate above that of low-viscosity fluids. According to the formula for jet injection power, $P = \frac{1}{8}\pi\rho D^2U^2$, where ρ is the fluid density, and D and U are the diameter and velocity of the microjet [27]. The lower injection speed of nanosuspensions may result in a slightly shallower injection depth and a relatively smaller distribution range compared to solutions. The overall therapeutic efficacy is ultimately reflected in the pharmacokinetic data.

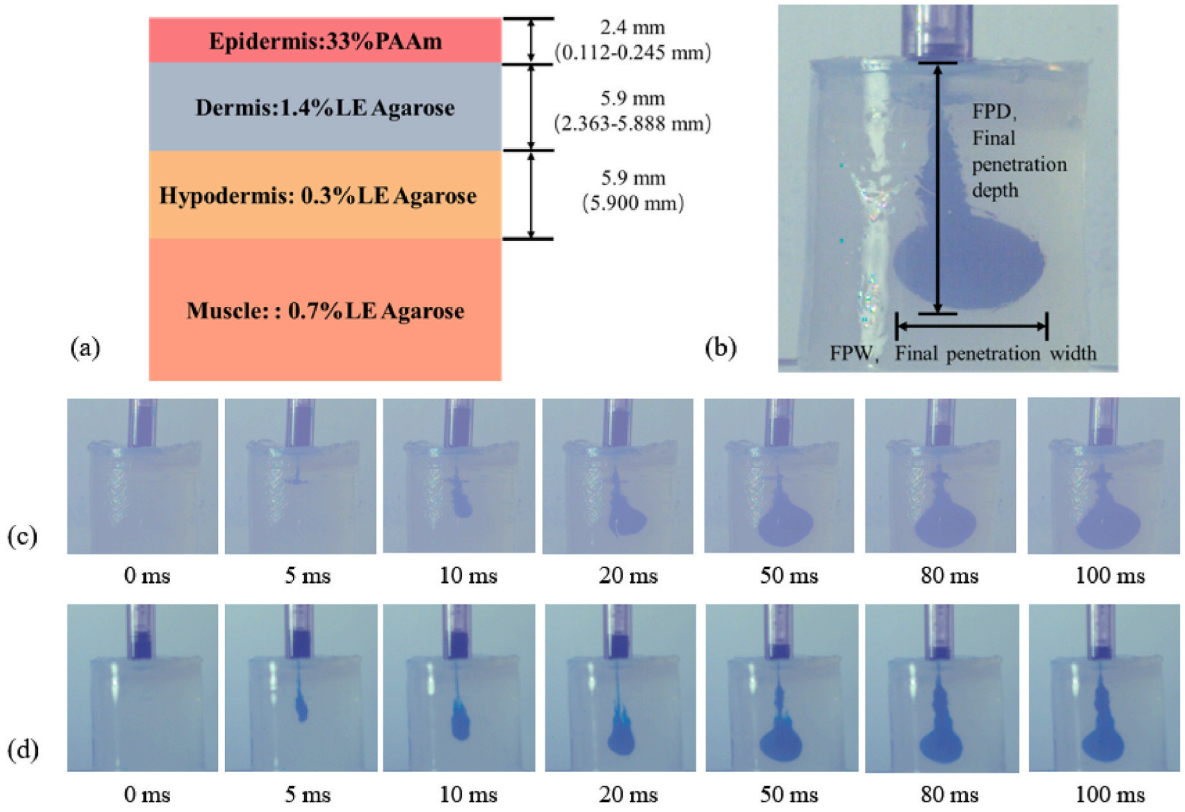

Fig. 4. Visualization of needle-free injection distribution in a muscular gel model. (a). schematic representation of the gel model's layers, (b) descriptive data of distribution with final penetration depth (FPD) and width (FPW) indicated, and illustration of the injection process of needle-free delivery for midazolam solution (c) and nanosuspension (d) at a volume of 0.2 mL.

3.2.2. Distribution within an injection phantom model

The distribution of intramuscularly injected drugs within tissues is a complex process influenced by various factors, including the injection site and depth, the physical and chemical properties of the drug, and interactions with the extracellular matrix (ECM). Researches indicated that following injection, drugs do not directly enter muscle cells but rather reside within the ECM, where the composition and structure significantly affect drug diffusion, stability, and subsequent absorption kinetics [31]. To simulate the behavior of drugs post-injection, a gel model that utilizing LE agarose and polyacrylamide have been developed to mimic different skin layers. This model, composed of layers representing the epidermis, dermis, subcutaneous, and muscle tissues as shown in Fig. 4 (a), was used to simulate NFIT with both the midazolam solution and nanosuspension. High-speed imaging techniques were employed to meticulously document the initial penetration and subsequent dispersion of the drug within this model.

Observations from the high-speed recordings indicated that the initial jet stream effectively penetrated through the simulated skin layers, reaching the muscle layer. The distribution was characterized by measuring the final penetration depth (FPD) and final penetration width (FPW), which is shown in Fig. 4b and Table 1. The results showed no significant difference in FPD and FPW between the solution and nanosuspension formulations, suggesting that both formulations achieved the intended depth of injection. Under the same injection volume conditions, no significant difference was observed in the FPD, ($P = 0.184 > 0.05$) and FPW ($P = 0.428 > 0.05$), indicating that the viscosity and density didn't influence the distribution range. When the injection volume was varied for the same formulation, the distribution difference was primarily evident in the FPW (Solution, $P = 0.002 < 0.05$; Nanosuspension, $P = 0.018 < 0.05$), suggesting that the injection volume significantly influences the lateral spread. The experimental results regarding the impact of delivery volume on the distribution of needle-free injections are consistent with existing findings [32]. Concurrently, our results demonstrated that the midazolam solution and nanosuspension formulations shows difference in the injection speed, yet they do not exert a significant impact on the distribution.

High-speed images in Fig. 4 (c) and (d) of the needle-free injection within a gel model revealed a process closely aligned with the stages of spring energy release, which can be divided into distinct phases: (1) an initial phase where the jet stream penetrates through the skin layers to reach the muscle layer; (2) a propagation phase during which the jet stream continues to be injected, spreading laterally and deepening within the muscle tissue; and (3) a terminal phase at the end of injection where further diffusion within the muscle tissue ceases, and the jet stream disperses within the dermis before filling the subcutaneous layer and injection channel to finalize the injection sequence.

In the study of in vitro distribution of needle-free injection technology, researchers have established various models to assess drug distribution and injection efficacy, including gelatin [33], polyacrylamide gel [34], and animal and human tissue models [28]. These models are crucial for understanding the initial interactions between drugs and muscle tissues, drug penetration depth, and the spatial distribution of drugs after injection, thereby enhancing our understanding of the complex interactions between drugs, injection techniques, and physiological environments. Despite providing valuable insights, these models also have some limitations. For instance, while gel models can simulate the properties of different skin layers, they still cannot fully replicate the multilayered structure and interlayer interactions of real skin. Furthermore, although the material properties of gel models, such as storage modulus and pore size, can be controlled by adjusting the formulation, they still differ from those of real tissues, potentially leading to deviations between experimental results and in vivo conditions. Gel models often lack the biological activity of real skin tissues, such as cell metabolism and immune responses, and the porous elastic properties of real skin tissues are far more complex than those of gel models, which may significantly impact drug diffusion and distribution. Therefore, although these models have played important roles in research, they still need continuous improvement and optimization to more accurately reflect real physiological conditions.

Table 1
Distribution outcomes of midazolam solution and nanosuspension at different volumes. FPD: final penetration depth; FPW: final penetration width.

Volume	Midazolam solution		Midazolam nanosuspension	
	FPD/cm	FPW/cm	FPD/cm	FPW/cm
0.1 mL	3.35 ± 0.37	1.80 ± 0.20	3.01 ± 0.50	1.59 ± 0.16
0.2 mL	2.87 ± 0.51	2.14 ± 0.25	3.22 ± 0.17	2.27 ± 0.24

3.3. Impact of needle-free injection on nanocrystals' particle size, skin and tissue injury

To evaluate the impact of needle-free injection on the particle size of delivered nanocrystals and the injury to the injection site, including skin and muscle tissue.

3.3.1. Effects of needle-free injection on nanocrystal particle size

The particle size of the nanocrystals was measured using DLS before and post injection. The results indicated that the initial particle size was 187.63 ± 3.59 nm, and the particle size remained at 185.40 ± 1.47 nm after the needle-free injection with no significant changes observed ($n = 3$, $P > 0.05$), as shown in Fig. 5. The stability of nanocrystals post-injection suggests that the needle-free injection process, including the acceleration and high-velocity impact with the skin, has a negligible impact on particle size.

3.3.2. Effects of needle-free injection on skin integrity

Cryo-SEM was utilized to assess skin injury following both 29G needle injection and needle-free injection on newborn pig skin, as shown in Fig. 6. The needle-free injections of both the solution and nanosuspension formulations resulted in smaller injury diameters of 27.02 ± 0.82 μm and 28.04 ± 4.01 μm, respectively, and injury areas of approximately 520 μm^2 and 417 μm^2. In contrast, needle injection caused significant injury, with a mean diameter of 248.13 ± 25.52 μm and an injury area of approximately 38,800 μm^2.Cryo-SEM images also revealed that traditional needle injections, upon needle withdrawal, resulted in tissue retraction that caused the epidermal layer to seal, presenting a wrinkled appearance indicative of the pressure applied. This process can lead to secondary injury to the epidermis due to the needle's removal. In contrast, needle-free injections created a punctate injury characterized by a distinct hole-like morphology, which signifies

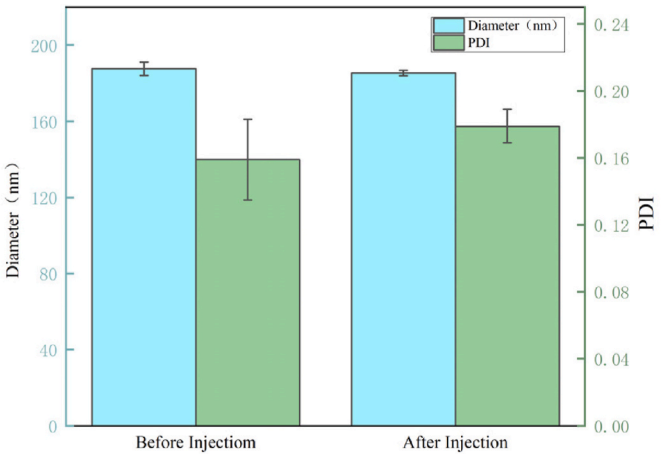

Fig. 5. Comparative particle size of nanocrystals before and post needle-free injection. The needle-free injection process has a negligible impact on particle size.

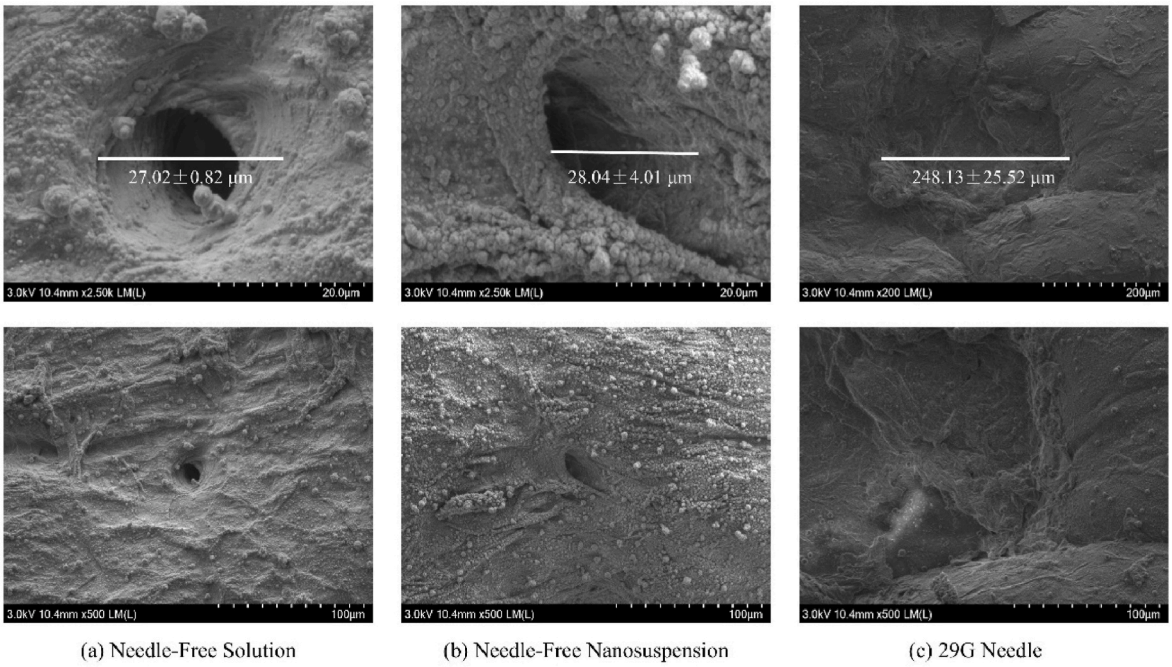

Fig. 6. Cryo-SEM images of skin injury induced by needle and needle-free injections. (a) needle-free injection of solution, (b) needle-free injection of nanosuspension, (c) 29G needle.

minimal tissue disruption. Importantly, these holes from needle-free injections may be filled with exudate and the injected medication. Conversely, the withdrawal of a needle can result in a vacuum effect, causing further damage to the tissues.

Given the inherent limitations of our experimental model, our study utilized excised porcine skin, which, despite its common use as a surrogate for human skin, exhibits differences in thickness, elastic modulus, and hair follicle distribution. These disparities may influence the assessment of tissue damage caused by needle-free injection. Furthermore, while Cyro-SEM provided valuable insights into surface and near-surface tissue damage, it is limited in its ability to fully capture deeper tissue alterations. Consequently, the observed reduction in tissue damage associated with needle-free injection should be interpreted with caution and in conjunction with the potential for intramuscular tissue damage.

3.3.3. *Effects of needle-free injection on muscle tissue*

The visualization of midazolam crystal distribution within muscle tissue is complex, primarily due to the drug's variable solubility in solvents and the potential for dissolution during tissue processing, such as the use of dehydrating agents in HE staining samples, which can alter the midazolam's presence.

To evaluate the impact of needle and needle-free injections on muscle tissue irritation, we employed these two injection methods to deliver saline and 1.7 % acetic acid solution, respectively. The HE staining results are shown in Fig. 7. Compared to the negative control group, no significant pathological change was observed after saline injection, suggesting that needle and needle-free injections have minimal effects on muscle tissue. Furthermore, to amplify the effects of different injection methods on muscle tissue, we administered 1.7 % acetic acid solution using both methods. The results indicated that the needle injection group exhibited significant muscle fascicle widening and muscle fiber degeneration, characterized by diffuse atrophy and degeneration across multiple muscle fascicles. The interstitial structures between some muscle fascicles were indistinct, and there was an increase in fibrous tissue within these fascicles. In contrast, the tissue damage in the

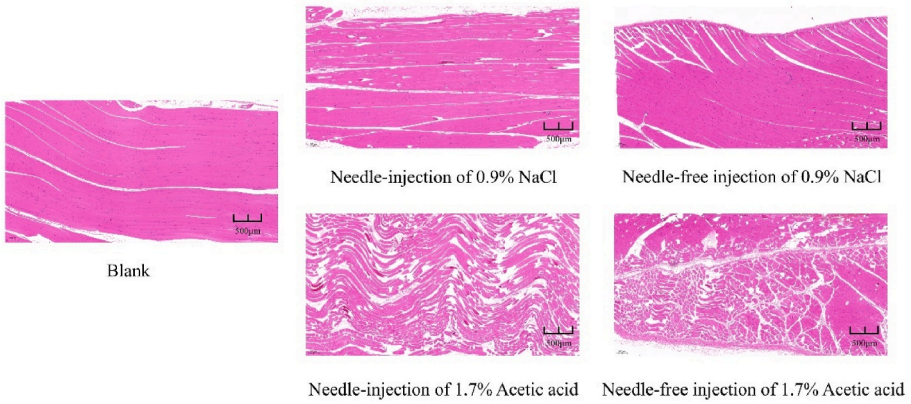

Fig. 7. The HE staining results of muscle tissue injury induced by needle and needle-free injections. The needle injection group exhibited significant muscle fascicle widening and muscle fiber degeneration, while the tissue injury in the needle-free injection group was relatively mild. The irritation caused by needle-free injection is lower than that of needle injection.

needle-free injection group was relatively mild. This may be because needle-free injection results in a more widespread distribution of the materials within the tissue, thereby reducing the local concentration. Our experimental results are consistent with previous studies [31,35], showing that substances delivered by both injection methods distribute along the interfascial planes of skeletal muscles, dispersing in the ECM between fibers and fascicles. The needle-free injection method, characterized by providing higher injection pressure and an initial diffuse distribution, results in a more widespread dispersion of the delivered drug at the injection site within muscle tissue. Therefore, the irritation caused by needle-free injection is lower than that of needle injection.

3.4. Pharmacokinetic

The SD rats were randomly divided into four groups which were administered by four treatments at a dose of 1 mg/kg, including injection of needle solution (N-S), needle-free solution (NF-S), needle nanosuspension (N-N), and needle-free nanosuspension (NF-N). The resulting plasma concentration-time profiles are depicted in Fig. 8 (a). The pharmacokinetic parameters are presented in Table 2. A strong linear correlation (r = 0.999) was established between the plasma concentration of midazolam (C) and the analytical ratio of the midazolam to the internal standard diazepam peak area ($X = A_{MD}/A_{DZ}$). This relationship was accurately quantified by the linear regression equation C = 419.323X+11.676 within a calibration range of 10–400 ng/mL.

Pharmacokinetic parameters, including C_{max}、$T_{1/2}$、CL、$AUC_{(0-t)}$, revealed no significant difference among the four administration methods, suggesting equivalent efficacy in delivering midazolam to the muscle tissue.

As illustrated in Fig. 8 (b), a notable distinction in T_{max} was observed. Specifically, the NF-N group exhibited significantly faster drug absorption, achieving a T_{max} of 11.67 ± 5.16 min, compared to 32.50 ± 22.08 min for the N-N group (P = 0.008 < 0.05) and 32.50 ± 14.75 min for the NF-S group (P = 0.048 < 0.05). Although it is generally expected that solutions would have a smaller T_{max} compared to nanosuspensions due to the immediate availability of midazolam in its molecular form for absorption, our findings indicate a different trend. This discrepancy is due to midazolam's poor solubility [36]. Despite achieving a higher solubility (50 mg/mL) using organic solvents like ethanol and mPEG350, the drug precipitates upon injection into muscle, forming larger particles. This results in a slower absorption process for the solution formulation, leading to a later T_{max} compared to the nanosuspension.

Analysis of the mean residence time ($MRT_{(0-t)}$) further revealed that the NF-N group had an extended MRT relative to the N-N group (P = 0.023 < 0.05). These findings indicate that, when delivering nanocrystals via needle-free injection, the absorption rate of midazolam is significantly enhanced and the residence time of the nanocrystals is prolonged. Notably, the T_{max} of the NF-N group was significantly shorter than that of Zeneo midazolam (approximately 48.9 min) [37]. Additionally, the plasma concentration-time curves for the NF-N group exhibited a more stable profile with less fluctuation, suggesting a more consistent therapeutic effect over time, despite no significant differences in $AUC_{(0-t)}$.

The pharmacokinetic profiles of drugs administered via NFIT vary depending on the formulation type, with solution formulations typically exhibiting an increase in C_{max} and a decrease in $MRT_{(0-t)}$. This may be primarily due to the fact that NFIT provides a diffuse distribution in tissues, allowing the solution to be more evenly distributed and providing a more consistent absorption pattern, leading to a higher peak plasma concentration. In contrast, after dispersion of nanocrystals, the smaller particles dissolve first, providing a faster absorption rate, while the larger particles dissolve slowly, offering a more sustained release due to their varying particle sizes. This is reflected as a faster T_{max}, a lower C_{max}, and a longer $MRT_{(0-t)}$ compared to the solution. These results support the notion that integrating NFIT with nanocrystals offers a superior strategy for enhancing drug delivery efficacy.

4. Conclusion and outlook

The current study marks an advancement in the field by showcasing the synergistic effects of NFIT utilized with midazolam in both solution and nanosuspension. Our analysis reveals that nanocrystal technology is pivotal for the efficient delivery of poorly water-soluble drugs that demand expedited therapeutic action. The integration of nanocrystals not only surmounts volume constraints but also augments drug solubility, accelerates the onset of action, and enhances bioavailability, thereby extending the applicative range of NFIT.

Our systematic evaluation has also confirmed that NFIT preserves the physicochemical integrity of nanocrystals post-injection, maintaining their size, which is crucial for understanding the mechanics of needle-free intramuscular injections. This finding deepens our understanding

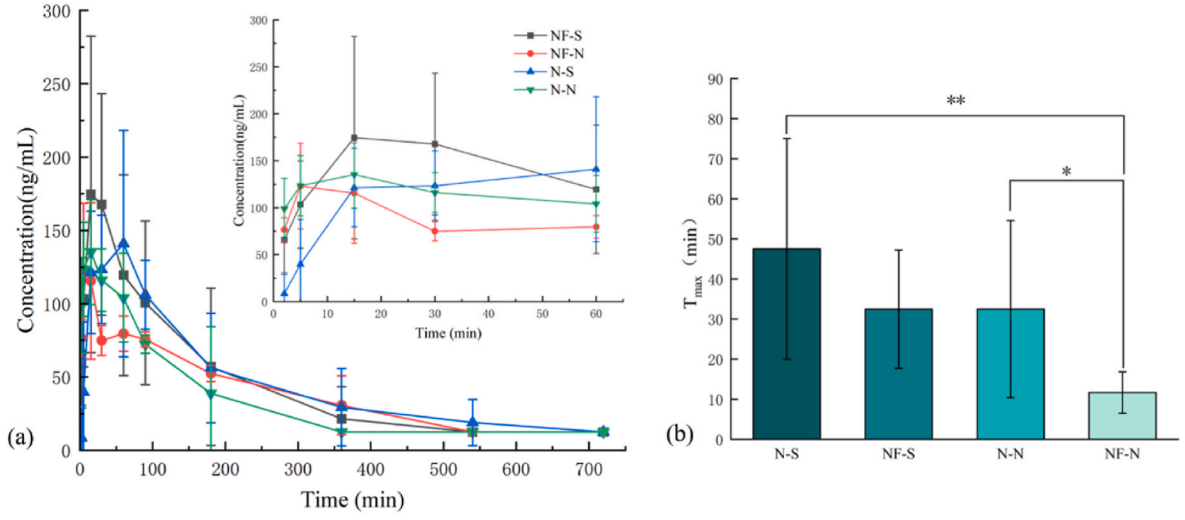

Fig. 8. Pharmacokinetic profiles of different treatment groups. NF-S: needle-free injection of midazolam solution; NF-N: needle-free injection of midazolam nanosuspension; N–S: needle injection of midazolam solution; N–N: needle injection of midazolam nanosuspension. (a) plasma concentration-time profiles, (b) comparative T_{max} of different groups. The NF-N group exhibited significantly faster drug absorption, achieving a T_{max} of 11.67 ± 5.16 min, compared to 32.50 ± 22.08 min for the N-N group (P = 0.008 < 0.05) and 32.50 ± 14.75 min for the NF-S group (P = 0.048 < 0.05).

Table 2
Pharmacokinetic parameters for each treatment group.

Parameters	Unit	N-S	NF-S	N-N	NF-N
T_{max}	min	47.50 ± 27.52	32.50 ± 14.75	32.50 ± 22.08	11.67 ± 5.16
C_{max}	ng/mL	156.70 ± 66.49	214.19 ± 97.35	147.30 ± 25.94	134.00 ± 53.72
$T_{1/2}$	h	3.99 ± 0.72	3.56 ± 0.82	4.04 ± 1.17	3.74 ± 0.28
CL	mL/h	0.44 ± 0.14	0.46 ± 0.14	0.55 ± 0.11	0.49 ± 0.06
$AUC_{(0-t)}$	h·ng/mL	542.82 ± 198.29	522.38 ± 188.43	396.75 ± 119.77	450.76 ± 58.97
$MRT_{(0-t)}$	h	3.43 ± 0.50	3.05 ± 0.55	3.16 ± 0.18	3.61 ± 0.37

of the injection process and its impact on drug delivery. Pharmacokinetic results have demonstrated that the combination of NFIT with nanocrystals significantly accelerates drug absorption, while minimizing skin injury, presenting a less invasive and more efficacious method of drug delivery. Future studies should delve into the cellular and molecular mechanisms underlying the synergistic effects of needle-free injections with nanocrystalline drug formulations to fully elucidate their therapeutic potential and functional dynamics.

In conclusion, the integration of NFIT with nanocrystal formulations presents a promising avenue for enhancing intramuscular drug delivery, offering a less invasive, more patient-compliant and rapidly effective approach to administer poorly water-soluble drugs like midazolam.

CRediT authorship contribution statement

He Zhang: Writing – original draft, Methodology, Formal analysis, Data curation. **Jiarui Chen:** Writing – original draft, Methodology, Formal analysis, Data curation. **Xiaolu Han:** Data curation. **Liang Xu:** Data curation. **Zengming Wang:** Writing – review & editing. **Nan Liu:** Writing – review & editing. **Yang Yang:** Supervision, Funding acquisition, Conceptualization. **Hui Zhang:** Supervision, Funding acquisition, Conceptualization. **Ai-ping Zheng:** Supervision, Funding acquisition, Conceptualization.

Declaration of generative AI and AI-assisted technologies in the writing process

During the preparation of this work, the authors used Kimi.ai to enhance the translation and linguistic expression of the paper. After using this tool, the authors reviewed and edited the content as needed and take full responsibility for the content of the publication.

Funding

This work was supported by National Key R&D Program of China (2023YFC2706100).

Declaration of competing interest

The authors declare that they have no known competing financial interests or personal relationships that could have appeared to influence the work reported in this paper.

Data availability

Data will be made available on request.

References

[1] D.A. Mengistu, S.T. Tolera, Y.M. Demmu, Worldwide prevalence of occupational exposure to needle stick injury among healthcare workers: a systematic review and meta-analysis, Can. J. Infect. Dis. Med. Microbiol. 2021 (2021) 9019534, https://doi.org/10.1155/2021/9019534.

[2] J. Schoppink, D. Fernandez Rivas, Jet injectors: perspectives for small volume delivery with lasers, Adv. Drug Deliv. Rev. 182 (2022) 114109, https://doi.org/10.1016/j.addr.2021.114109.

[3] R. Chapman, M. Van Diepen, N. Douglass, T. Hermanus, P.L. Moore, A. L. Williamson, Needle-free devices and CpG-adjuvanted DNA improve anti-HIV antibody responses of both DNA and modified vaccinia ankara-vectored candidate vaccines, Vaccines 11 (2023), https://doi.org/10.3390/vaccines11020376.

[4] S. Mao, S. Li, Y. Zhang, L. Long, J. Peng, Y. Cao, J.Z. Mao, X. Qi, Q. Xin, G. San, J. Ding, J. Jiang, X. Bai, Q. Wang, P. Xu, H. Xia, L. Lu, L. Xie, D. Kong, S. Zhu, W. Xu, A highly efficient needle-free-injection delivery system for mRNA-LNP vaccination against SARS-CoV-2, Nano Today 48 (2022) 101730, https://doi.org/10.1016/j.nantod.2022.101730.

[5] Y.P. D, K. Sanjay, A. Kshitij, J. Mukul, P.D. R, M. Kapil, M. Basavaraj, G. Suresh, M. Sreelekshmy, S. Anita, S. Gajanan, P.D. Y, D. Ayan, C. Harish, D. Gururaj, G. Nivedita, A. Priya, K. Himanshu, S.R. R, T. Anuradha, N. Dimpal, J. Rajlaxmi, K. Abhimanyu, S. Prasad, B. Shreekant, R. Chozhavel, R.H. Prasad, P. Satish, S. Niraj, D. Pankaj, S. Dharmendra, Needle-free injection system delivery of ZyCoV-D DNA vaccine demonstrated improved immunogenicity and protective efficacy in Rhesus macaques against SARS-CoV-2, J. Med. Virol. 95 (2023).

[6] Q. Pan, L. Zhang, A. Gu, D. Yu, X. Wang, Y. Zhou, L. Guo, The absorption of needle-free insulin aspart through jet injector in different body parts of healthy individuals, Front. Endocrinol. 13 (2022) 832726, https://doi.org/10.3389/fendo.2022.832726.

[7] F. Sun, B. Gao, A. Yang, L. Ren, Y. Xing, K. Ma, L. Tian, S. Li, C. Heng, H. Liu, J. Zhou, Q. Ji, Needle-free injection of basal insulin improves fasting glucose variability as assessed by continuous glucose monitoring in T2DM: a prospective randomized multicenter open-label crossover study, Expet Opin. Drug Deliv. (2022) 1–10, https://doi.org/10.1080/17425247.2022.2147504.

[8] F. Sun, B. Gao, A. Yang, L. Ren, Y. Xing, K. Ma, L. Tian, S. Li, C. Heng, H. Liu, J. Zhou, Q. Ji, Needle-free injection of basal insulin improves fasting glucose variability as assessed by continuous glucose monitoring in T2DM: a prospective randomized multicenter open-label crossover study, Expet Opin. Drug Deliv. 19 (2022) 1725–1734, https://doi.org/10.1080/17425247.2022.2147504.

[9] A. Beisti Ortego, C. Fuertes Rodrigo, M. Ferrer Lozano, J.I. Labarta Aizpun, A. De Arriba Muñoz, Adult height in short children born small for gestational age treated with growth hormone, Med. Clin. 154 (2020) 289–294, https://doi.org/10.1016/j.medcli.2019.06.005.

[10] M. Michaelidou, S. Whitten, P. Bajaj, A. Knight, H.A. Spoudeas, Improved adherence and growth outcomes with jet-delivered growth hormone, J. Pediatr. Endocrinol. 32 (2019) 207–213, https://doi.org/10.1515/jpem-2018-0067.

[11] J.F. Hernandez-Franco, Y.C. Mosley, J. Franco, D. Ragland, Y. Yao, H. Hogenesch, Effective and safe stimulation of humoral and cell-mediated immunity by intradermal immunization with a cyclic dinucleotide/nanoparticle combination adjuvant, J. Immunol. 206 (2021) 700–711, https://doi.org/10.4049/jimmunol.2000703.

[12] R.J. Mumper, Z. Cui, Genetic immunization by jet injection of targeted pDNA-coated nanoparticles, Methods 31 (2003) 255–262, https://doi.org/10.1016/s1046-2023(03)00138-5.

[13] S. Hu, Z. Li, J. Cores, K. Huang, T. Su, P.U. Dinh, K. Cheng, Needle-free injection of exosomes derived from human dermal fibroblast spheroids ameliorates skin photoaging, ACS Nano 13 (2019) 11273–11282, https://doi.org/10.1021/acsnano.9b04384.

[14] M. Schlich, F. Lai, S. Murgia, D. Valenti, A.M. Fadda, C. Sinico, Needle-free jet injection of intact phospholipid vesicles across the skin: a feasibility study, Biomed. Microdevices 18 (2016) 67, https://doi.org/10.1007/s10544-016-0098-3.

[15] C.H. Park, L.D. Tijing, C.S. Kim, K.M. Lee, Needle-free transdermal delivery using PLGA nanoparticles: effect of particle size, injection pressure and syringe orifice diameter, Colloids Surf. B Biointerfaces 123 (2014) 710–715, https://doi.org/10.1016/j.colsurfb.2014.10.009.

[16] M. Schlich, L. Casula, A. Musa, R. Pireddu, G. Pitzanti, M.C. Cardia, D. Valenti, S. Marceddu, A.M. Fadda, M.A. De Luca, C. Sinico, F. Lai, Needle-free jet injectors and nanosuspensions: exploring the potential of an unexpected pair, Pharmaceutics 14 (2022), https://doi.org/10.3390/pharmaceutics14051085.

[17] S. Mao, S. Li, Y. Zhang, L. Long, J. Peng, Y. Cao, J.Z. Mao, X. Qi, Q. Xin, G. San, J. Ding, J. Jiang, X. Bai, Q. Wang, P. Xu, H. Xia, L. Lu, L. Xie, D. Kong, S. Zhu, W. Xu, A highly efficient needle-free-injection delivery system for mRNA-LNP vaccination against SARS-CoV-2, Nano Today 48 (2023) 101730, https://doi.org/10.1016/j.nantod.2022.101730.

[18] M. Schlich, L. Casula, A. Musa, R. Pireddu, G. Pitzanti, M.C. Cardia, D. Valenti, S. Marceddu, A.M. Fadda, M.A. De Luca, C. Sinico, F. Lai, Needle-free jet injectors and nanosuspensions: exploring the potential of an unexpected pair, Pharmaceutics 14 (2022) 1085.

[19] S.P. Nordt, R.F. Clark Midazolam, A review of therapeutic uses and toxicity. J. Emerg, Médica Sur 15 (1997) 357–365, https://doi.org/10.1016/s0736-4679(97)00022-x.

[20] P.E. Penovich, V.R. Rao, L. Long, E. Carrazana, A.L. Rabinowicz, Benzodiazepines for the treatment of seizure clusters, CNS Drugs 38 (2024) 125–140, https://doi.org/10.1007/s40263-023-01060-1.

[21] J. Kadel, S. Bauer, A.M. Hermsen, I. Immisch, L. Kay, K.M. Klein, S. Knake, K. Menzler, P.S. Reif, F. Rosenow, A. Strzelczyk, Use of emergency medication in adult patients with epilepsy: a multicentre cohort study from Germany, CNS Drugs 32 (2018) 771–781, https://doi.org/10.1007/s40263-018-0544-2.
[22] K.A. Owusu, M.B. Dhakar, C. Bautista, D. Mckimmy, S. Cotugno, N. Sukumar, Y. Deng, P. Farooque, L.J. Hirsch, C.B. Maciel, Comparison of intranasal midazolam versus intravenous lorazepam for seizure termination and prevention of seizure clusters in the adult epilepsy monitoring unit, Epilepsy Behav. 98 (2019) 161–167, https://doi.org/10.1016/j.yebeh.2019.07.021.
[23] M. Maltseva, F. Rosenow, F. Von Podewils, L. Habermehl, L. Langenbruch, L. Bierhansl, S. Knake, J. Schulz, B. Gaida, L. Kämppi, C. Mann, A. Strzelczyk, Predictors for and use of rescue medication in adults with epilepsy: a multicentre cross-sectional study from Germany, Seizure 118 (2024) 58–64, https://doi.org/10.1016/j.seizure.2024.04.005.
[24] D. Patel, S.S. Zode, A.K. Bansal, Formulation aspects of intravenous nanosuspensions, Int. J. Pharm. 586 (2020) 119555, https://doi.org/10.1016/j.ijpharm.2020.119555.
[25] M.B. Mcguckin, J. Wang, R. Ghanma, N. Qin, S.D. Palma, R.F. Donnelly, A. J. Paredes, Nanocrystals as a master key to deliver hydrophobic drugs via multiple administration routes, J. Contr. Release 345 (2022) 334–353, https://doi.org/10.1016/j.jconrel.2022.03.012.
[26] A. Mohizin, D. Lee, J.K. Kim, Impact of the mechanical properties of penetrated media on the injection characteristics of needle-free jet injection, Exp. Therm. Fluid Sci. 126 (2021) 110396, https://doi.org/10.1016/j.expthermflusci.2021.110396.
[27] M. Abdul, K. Jung Kyung, K. Jung Kyung, Current engineering and clinical aspects of needle-free injectors: a review, J. Mech. Sci. Technol. (2018) 5737–5747, https://doi.org/10.1007/s12206-018-1121-9.
[28] J. Seok, C.T. Oh, H.J. Kwon, T.R. Kwon, E.J. Choi, S.Y. Choi, S.K. Mun, S.-H. Han, B.J. Kim, M.N. Kim, Investigating skin penetration depth and shape following needle-free injection at different pressures: a cadaveric study, Laser Surg. Med. 48 (2016) 624–628, https://doi.org/10.1002/lsm.22517.
[29] R. Mauludin, R.H. Müller, C.M. Keck, Kinetic solubility and dissolution velocity of rutin nanocrystals, Eur. J. Pharmaceut. Sci. 36 (2009) 502–510, https://doi.org/10.1016/j.ejps.2008.12.002.
[30] J. William Mckeage, H. Janet Full, A. Zheng Hao Tan, A. James Taberner, The effect of temperature-dependent drug viscosity on needle-free jet injection, Int. J. Pharm. 666 (2024) 124777, https://doi.org/10.1016/j.ijpharm.2024.124777.
[31] A.J.S. Mccartan, D.W. Curran, R.J. Mrsny, Evaluating parameters affecting drug fate at the intramuscular injection site, J. Contr. Release 336 (2021) 322–335, https://doi.org/10.1016/j.jconrel.2021.06.023.
[32] K. Chen, H. Zhou, J. Li, G.J. Cheng, A model on liquid penetration into soft material with application to needle-free jet injection, J. Biomech. Eng. 132 (2010) 101005, https://doi.org/10.1115/1.4002487.
[33] P. Rohilla, J.O. Marston, In-vitro studies of jet injections, Int. J. Pharm. 568 (2019) 118503, https://doi.org/10.1016/j.ijpharm.2019.118503.
[34] A. Schoubben, A. Cavicchi, L. Barberini, A. Faraon, M. Berti, M. Ricci, P. Blasi, L. Postrioti, Dynamic behavior of a spring-powered micronozzle needle-free injector, Int. J. Pharm. 491 (2015) 91–98, https://doi.org/10.1016/j.ijpharm.2015.05.067.
[35] A.L. Daugherty, R.J. Mrsny, Local tissue distribution and cellular fate of vascular endothelial growth factor (VEGF) following intramuscular injection, J. Drug Target. 18 (2010) 27–35, https://doi.org/10.3109/10611860903134317.
[36] L.B. Pfendt, T.J. Janjić, G.V. Popović, Study of protolytic, hydrolytic and solubility equilibria of midazolam, Analyst 120 (1995) 2145–2151, https://doi.org/10.1039/AN9952002145.
[37] O. Lacombe, Y. Pletan, J.-M. Grouin, A. Brennan, O. Giré, Relative bioavailability study of midazolam intramuscularly administered with the needle-free auto-injector ZENEO® in healthy adults, Neurology and Therapy 13 (2024) 1155–1172, https://doi.org/10.1007/s40120-024-00627-4.